Modelling the internal stress field in argillaceous rocks under humidification/desiccation

Linlin Wang, Amade Pouya, Michel Bornert, Bernard Halphen

Modelling the internal stress field in argillaceous rocks under humidification/desiccation

L.L. Wang[1], A. Pouya[2,*,†], M. Bornert[2] and B. Halphen[3]

[1]Laboratoire de Mécanique des Solides (UMR 7649), Ecole Polytechnique, 91128 Palaiseau, France
[2]Laboratoire Navier (UMR 8205), CNRS, ENPC, IFSTTAR, Université Paris-Est, 77455 Marne-la-Vallée, France
[3]Sétra, 77487 Provins, France

This paper deals with analytical and numerical modelling of the internal stress generated in argillaceous rocks during humidification/desiccation processes, which is an essential issue for damage study. This local stress field arises from two mechanisms: (i) complex interactions between free swelling/shrinking clay matrix and non-strained inclusions of carbonate and quartz and (ii) a self-restraint effect induced by the moisture gradient during the transient moisture exchange process. The inclusion–matrix interaction is investigated in different cases. Firstly, the analytical solution of the stress around a cylindrical inclusion embedded in an infinite swelling matrix is derived: The inclusion would suffer tension (compression) under humidification (desiccation), and the resulting cracking patterns are discussed. Then, the problem of two inclusions with different distances in an infinite swelling matrix is considered, and it is shown that the local stress around an inclusion will be perturbed and amplified by neighbouring inclusions. Finally, an inclusion outcropping at the free surface of a swelling matrix is modelled as to investigate the effect of free surface: The inclusion–matrix interface undergoes shear stresses of which the maximum is found at the free surface. In addition to the inclusion–matrix interaction, the self-restraint effect is investigated: The induced stress is maximal at the beginning of humidification/desiccation processes and vanishes gradually with time. The quantity of the self-restraint stress is strongly controlled by the hydric loading rate.

KEY WORDS: argillaceous rocks; humidification/desiccation; inclusion–matrix interaction; self-restraint effect

1. INTRODUCTION

Argillaceous rocks are intensively studied as possible host rocks for underground radioactive nuclear waste disposal in the last decades. During different stages of the service life, such rocks are subjected to some humidification/desiccation processes that may lead to damage phenomena [1, 2]. These damage phenomena modify the permeability of the host rock and are unfavourable for the sealing of a long-term repository [3–5].

The experimental observations have evidenced microcracks emerging in both humidification and desiccation cases [6, 7]. Apparition of these microcracks is linked to different restraints that can generally be classified into two types: external and internal restraints. The external restraint is related to the external mechanical loading and the substrate-restraint effect. The internal restraint for argillaceous rocks consists of two terms: (i) inclusion–matrix interaction and (ii) self-restraint effect. The argillaceous rock is a heterogeneous material, made of numerous inclusions (mostly carbonate and quartz) scattered in a continuous clay matrix. Because of its specific physicochemical properties,

*Correspondence to: A. Pouya, Laboratoire Navier (ENPC-IFSTTAR-CNRS), Université Paris-Est
†E-mail: Ahmad.Pouya@enpc.fr

the clay matrix tends to swell (shrink) under humidification (desiccation). However, this free deformation is inhibited by the non-strained inclusions, and some local stresses are generated. The stress induced by inclusion–matrix interaction is controlled by the free swelling quantity, the morphology, and the mechanical properties of the inclusions and the matrix [8, 9]. A moisture gradient develops inside the specimen during the transient moisture transport stage. Hence, the inner part of samples inhibits the swelling/shrinking of the outer part, and this is the second mechanism of internal stresses. The stress induced by moisture gradient, commonly called self-restraint effect, is governed by the specimen geometry as well as the hydric loading rate, etc. The self-restraint effect is responsible for the shrinkage (by drying or cooling)-induced cracking that can be found in a wide range of materials [10–13].

This paper focuses on the internal restraint (without external restraint) of argillaceous rocks under humidification/desiccation. The material is considered as a matrix–inclusion composite, in which the clay matrix swells (shrinks) freely (without mechanical stress) when the relative humidity (RH) varies. This paper is composed of two parts. The first part addresses the mathematical formulation: The constitutive equation of argillaceous rocks under humidification/desiccation is derived, as well as a simplified model of humidification (desiccation) process that is necessary for studying the self-restraint effect. The second part focuses on the internal stress field generated by the two terms of internal restraint: inclusion–matrix interaction and self-restraint effect. Different cases are considered: one cylindrical inclusion and two inclusions with variable distances embedded in a swelling matrix and a hemispheric inclusion outcropping at the free surface of a semi-infinite swelling matrix. The convention of the mechanics of a continuum medium is applied, that is, extension (tension) is considered to be positive for the strain (stress).

2. BEHAVIOUR OF ARGILLACEOUS ROCKS UNDER HUMIDIFICATION/DESICCATION

2.1. Governing equations under hydric loads

The behaviour of argillaceous rocks under humidification/desiccation is a coupled problem of physical chemistry and mechanics. Firstly, the clay mineral undergoes a volume variation because of RH change. This physicochemical response can be considered as a free deformation in the context of mechanics. Secondly, the non-swelling inclusions inhibit the swelling/shrinking of a clay matrix. Moreover, a moisture gradient develops inside the sample during the moisture transport process. The previously mentioned two terms lead to an internal stress field, which is responsible for the mechanical response. Based on the previously mentioned considerations, the equations governing the local behaviour of argillaceous rocks can be reasonably written in the following simple hydric-elastic form:

$$\boldsymbol{\sigma}(x) = \mathbb{C}(x) : \left[\boldsymbol{\varepsilon}(x) - \boldsymbol{\varepsilon}^{F}(x)\right] \tag{1}$$

where $\sigma(x)$ and $\varepsilon(x)$ are the local stress and strain at position x in the microstructure. The mechanical interactions are attributed to non-uniformity of the elastic stiffness tensor $C(x)$ and incompatibility of local free strains $\boldsymbol{\varepsilon}^{F}(x)$. It is noted that the free-strain-multiplied stiffness tensor gives a stress, so the right term of Eqn 1 is equivalent with a pre-stress that is usually met with in thermomechanical problems. Eqn 1 can also be considered as an 'effective stress' expression usually used in poromechanics in which liquid pressure corresponds to the 'free strain' term here.

Argillaceous rocks exhibit multiscale heterogeneity, and the clay matrix is also inhomogeneous because of various clay groups (smectite, illite and kaolinite) and distributed clay particle orientations. Because this study concerns the inclusion–matrix interaction, the intra-phase heterogeneity of the clay matrix is neglected here. In this case, the local stiffness tensor can be written as

$$\mathbb{C}(x) = \begin{cases} \mathbb{C}^M \text{in clay matrix} \\ \mathbb{C}^I \text{in inclusion} \end{cases} \tag{2}$$

Similarly, the local free strain can be written as

$$\boldsymbol{\varepsilon}^F(x) = \begin{cases} \boldsymbol{\varepsilon}^h(x) \text{in clay matrix} \\ 0 \text{ in inclusion} \end{cases} \tag{3}$$

The free strain in the matrix involves a physicochemical swelling $\boldsymbol{\varepsilon}^h$ of clay minerals with RH increase. Actually, the volume growth consists in separation of pore spaces on multiscales, controlled by different mechanisms: (i) crystalline swelling associated with the change of interlayer spacing as a result of hydration of water layers by interlayer cations, (ii) double-layer swelling related to separation of interparticle space by the effect of a diffuse double layer, and (iii) breakup of large clay particles into smaller ones, which results in a transition from interlayer spaces into interparticle spaces [14]. Moreover, the swelling of the clay matrix is also attributable to variation of capillary pressure as for all porous media. The swelling of the clay matrix can be considered as a function of RH:

$$\frac{d\boldsymbol{\varepsilon}^h}{dh_r} = \boldsymbol{H} \tag{4}$$

where h_r is the RH, and H is the swelling coefficient tensor of clay minerals. It is noted that a $\boldsymbol{\varepsilon}^h$–$h_r$ relationship is non-linear so as H is RH dependent: It is small at low RH, whereas it becomes significant at high RH, for example, the threshold is around 80% RH for Callovo-Oxfordian argillaceous rocks. Besides, H is anisotropic: The swelling is much more significant along the direction perpendicular to the orientation of clay particles [15]. Nevertheless, H is assumed to be constant and isotropic for simplicity in this study.

2.2. *Moisture transport model during humidification/desiccation*

The humidification/desiccation of a porous medium consists in a biphase movement: vapour diffusion that obeys Fick's law, as well as liquid water transport that is normally described by Darcy's law. Moreover, phase transition (condensation or evaporation) occurs simultaneously in a porous medium because of capillary effect. Broadly, the humidification (desiccation) process in a porous medium is achieved by two mechanisms: (i) a process of vapour diffusion followed by a water condensation (evaporation) inside the specimen and (ii) a process of liquid water transportation from (towards) the specimen boundary where vapour condensates (water evaporates). Coussy [16] has demonstrated that the moisture transport in weakly permeable materials (intrinsic permeability $K < 10^{-19}\,\mathrm{m}^2$) is conducted mainly in its liquid form, that to say, the second mechanism. This means that the effect of the vapour diffusion and the condensation within the sample can be ignored. The intrinsic permeability of Callovo-Oxfordian argillaceous rocks varies from 10^{-23} to $10^{-19}\,\mathrm{m}^2$, which is within the weakly permeable material range mentioned previously. For such case, a simplified diffusion equation can be used to describe the moisture transport process [17]:

$$\phi \frac{\partial S_l}{\partial t} + div(D_l grad S_l) = 0 \tag{5}$$

with

$$D_l = P_c^{'}(S_l) K_l = P_c^{'}(S_l) \frac{K k_{rl}(S_l)}{\eta_l}$$

where S_l is the degree of saturation, and ϕ and η_l denote the porosity of a porous medium and the dynamic viscosity of water, respectively. K is the intrinsic permeability of the porous material independent

of saturation, while k_{rl} is the relative permeability that is S_l dependent. For Callovo-Oxfordian argillaceous rocks, it can be expressed by the formula proposed by Bovet [18]:

$$k_{rl} = (S_l)^n \tag{6}$$

where $n = 3$ for the saturation case, and $n = 3.5$ for the desaturation case.

Recall that capillary pressure P_c is defined as the difference between gas pressure and water pressure ($P_c = P_g - P_w$). The P_c–S_l relationship is described by the isothermal water retention curve. Based on laboratory experimental data, a representative approximation based on the Vauclin–Vachaud relation has been chosen for the isothermal water retention curve of Callovo-Oxfordian argillaceous rocks [18]:

$$S_l = \frac{a}{a + (100P_c)^b} \tag{7}$$

where $a = 2842$ and $b = 0.906$ when P_c is expressed in MPa.

Supposing the gas pressure remains constantly equal to the atmosphere pressure (P_{atm}), the capillary pressure can be linked to the RH by the famous Kelvin's law:

$$\rho_l \frac{RT}{M_v} \ln(h_r) = P_c \tag{8}$$

where M_v, R, and T stand for the molar mass of water, ideal gas constant, and temperature, respectively. ρ_l is the mass density of water. Finally, the parameters describing the humidity state of specimen (h_r, P_c, S_l) are linked by Eqns 7 and 8.

The following investigation of the internal stress field is based on a humidification from 80% to 90% RH in the context of elasticity. The swelling coefficient of clay matrix is reasonably chosen to be constant as 10^{-2}/100%RH, that is, the free swelling of clay matrix $\varepsilon^h = 1 \times 10^{-3}$. The swelling coefficient is order compatible with the experimental data in the high RH range [19]; for low RH level, it will be much smaller so the internal stress will be more modest. The swelling of clay matrix is supposed isotropic for simplicity. One can deduce that the anisotropy of H may lead to a network of microcracking with a preferential orientation: It might be perpendicular to the direction of the major swelling. The matrix and inclusion are considered as homogeneous isotropic elastic materials, and their mechanical constants are chosen from data collected by Agence nationale pour la gestion des déchets radioactifs (ANDRA) [18] and listed in Table I.

3. INTERNAL STRESS FIELD UNDER HUMIDIFICATION/DESICCATION

3.1. A cylindrical inclusion embedded in an infinite swelling matrix

Consider an elastic cylinder (inclusion) embedded in an infinite homogeneous isotropic elastic medium (clay matrix) that undergoes a uniform isotropic swelling (Figure 1). It is assumed that the thickness of the sample in the z-direction is much smaller than in-plane dimensions, so the plane stress condition manifests itself. The cylindrical coordinates are used here. Because of the symmetry, all stress and

Table I. Reference values for the key parameters of Callovo-Oxfordian argillaceous rocks.

Notation	Parameter	Value
E_m	Young's modulus of the matrix	10 GPa
ν_m	Poisson's coefficient of the matrix	0.2
E_i	Young's modulus of the inclusion	80 GPa
ν_i	Poisson's coefficient of the inclusion	0.2
H	Swelling coefficient of the clay matrix	10^{-2}/100% RH
K	Intrinsic permeability	$10^{-20}\,\mathrm{m}^2$
η_l	Dynamic viscosity of water	$1.00 \times 10^{-3}\,\mathrm{Pa \cdot s}$
ρ_l	Volumetric mass of water	$1000\,\mathrm{kg\,m^{-3}}$
M	Molar mass of vapour	$1.8 \times 10^{-2}\,\mathrm{kg\,mol^{-1}}$
R	Ideal gas constant	$8.31\,\mathrm{J\,K^{-1}\,mol^{-1}}$
T	Temperature	293.8 K

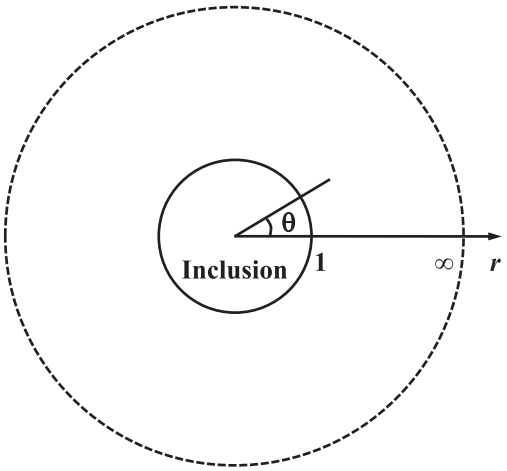

Figure 1. Geometry of the specimen with a cylindrical inclusion in an infinite clay matrix.

strain components are only r-dependent. The governing equations for this problem are the same as that for a thermoelastic problem except that the thermal expansion is replaced by the swelling deformation. These equations and their method of resolution are classical and have been recalled in the Appendix. The inclusion–matrix interaction results in uniform hydrostatic tension in the inclusion. The stress in the matrix is maximal at the interface and decreases in the order of r^{-2} with the distance from the inclusion centre: It is tensile radially and compressive in the orthoradial direction (Figure 2). No shear stress will be generated in this analysis because of rotational symmetry. The strain is

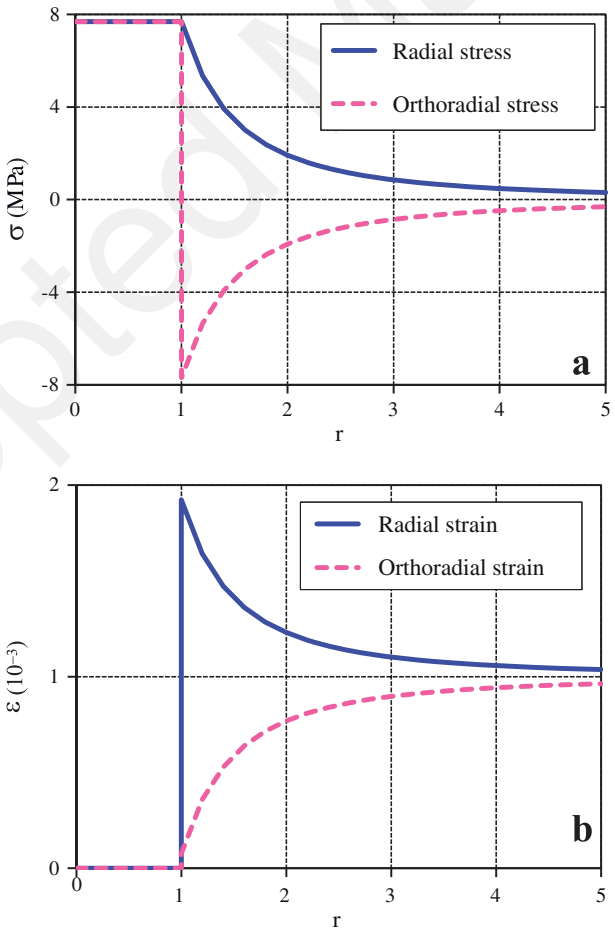

Figure 2. Evolution with r of the local stress (a) and strain (b) as a result of inclusion–matrix interaction under plane strain condition (inclusion radius is 1).

homogeneous in the inclusion 0.08×10^{-3}. The radial strain of the matrix at the interface is 2.3×10^{-3}, which is even greater than the free swelling 1×10^{-3}.

It is stressed that the original aim of this analysis relied on interpreting some observations of microcrackings during humidification/desiccation processes on thin samples [6]. Hence, plane stress condition is chosen in the present analysis; it can, however, be easily extended to other cases, and the conclusions will be similar except for quantitative differences. For example, considering always a cylindrical inclusion, the radial stress at the inclusion–matrix interface will be 9.3 MPa when the plane strain condition applies compared with 7.7 MPa for the stress plane condition, and it decreases in the order of r^{-2} with the distance from the inclusion centre. For a spherical inclusion, it will be 13.3 MPa at the interface and decreases in the order of r^{-3} with the distance.

The previously mentioned problem can be considered with the help of a set of imaginary cutting, straining and welding operation, shown in Figure 3. At the initial state, the inclusion (circle) and matrix (circular ring) adhere well with each other. Then, cut around the inclusion and remove it from the matrix. Allow a non-constraint swelling of the matrix to take place. It should be noted that the swelling results in an increase of the inner diameter of the circular ring. Finally, put the inclusion back in the matrix and rejoin it across the cut. The adhesion of a non-swelling inclusion hinders the growth of the hole in the matrix and consequently results in tension at the interface.

3.1.1. Microcrack patterns under humidification/desiccation. Evaluating the internal stress field has a great interest for damage study. The tensile strength of Callovo-Oxfordian argillaceous rocks is about 3 MPa, while their compressive strength is 21 MPa [18]. Note that these reference values, obtained by Brazilian tension and uniaxial compression tests, are macroscopic parameters. However, the study on microcracking here requires microscopic parameters of three elements (inclusions of carbonate and quartz, clay matrix and their interfaces) that are greatly contrasting. The inclusions are relatively stiff and own high strengths, for example, the tensile strength of quartz is 48 MPa, while its compressive strength can attain 1.1 GPa. Damage occurs more easily in the clay matrix or at the inclusion–matrix interface. Unfortunately, the mechanical resistances for these two parts are extremely lacking. Therefore, only qualitative analysis on potential dangerous positions and likely microcrack patterns are discussed in the following.

For the humidification case, the maximum tensile stress is the radial stress at the interface. If its value exceeds the inclusion–matrix bond strength, a separation of the inclusion from the clay matrix occurs (Figure 4a). If the tensile strength of the clay matrix is even lower than the inclusion–matrix cohesion, a tensile failure takes place in the immediate vicinity of the interface. The crack pattern, in this case, is similar to the previous one, only now the inclusion is covered by a thin layer of clay.

In case of desiccation, the stress distribution is similar to that under humidification but with opposite sign. The tensile orthoradial stress potentially creates microcracks that radiate from the interface into the clay matrix (Figure 4b). Consequently, shear stress is generated along the interface, and its extent attains the maximum near the radial cracks. This might result in shear microcracks at the inclusion boundaries.

As a summary, the interaction between the free-strained clay matrix and inclusions results in a local stress field, which is a potential source of damage. The maximum is always located at the inclusion–matrix interface, regardless whether it undergoes humidification or desiccation. However, the possible

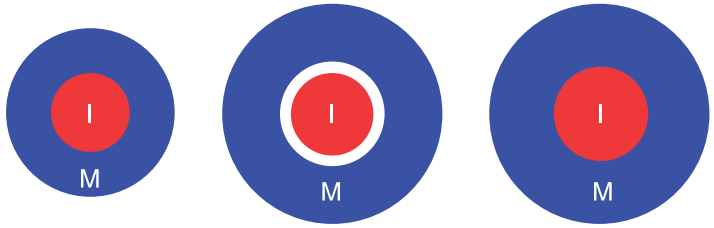

Figure 3. Interaction between the inclusion and the swelling matrix.

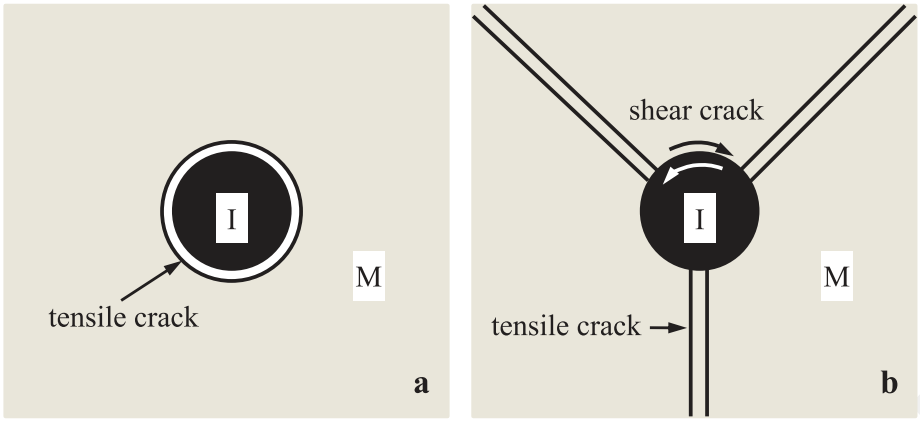

Figure 4. Potential microcrack patterns in case of (a) swelling matrix and (b) shrinking matrix.

microcrack patterns are dissimilar for the two cases: Humidification possibly results in tensile failure along the inclusion–matrix interface, whereas radial cracks may occur in the clay matrix under desiccation together with shear cracks along the interface.

3.2. Two cylindrical inclusions embedded in a swelling matrix

The previous modelling concerns an inclusion in an infinite matrix, and so, only the inclusion–matrix interaction is considered. The internal stress field in argillaceous rocks is, however, also controlled by the interactions between the inclusions. To study these interactions, a case of two circular inclusions (with uniform diameter $d = 0.5$) embedded in a free-swelling matrix is modelled, always in the plane stress condition. Because the interaction is strongly controlled by the distance between the inclusions, various D values (distance between the centres of two inclusions) are studied. The Porofis (software for the finite element analysis of fissured porous media developed by Pouya, 2010) is used for the calculation. The size of the matrix (20 times the inclusion diameter) is chosen large enough to represent the field condition as an infinite boundary (Figure 5). The stress maps for the $D = 1.2d$ case, shown in Figure 6, reveal that the stress field around an inclusion is strongly perturbed by the neighbouring one, especially in its front side and the matrix between the inclusions. The homogeneous stress field for the one inclusion case becomes heterogeneous, and their magnitude becomes more important: The maximum values for principal stresses (σ_1 and σ_3) are

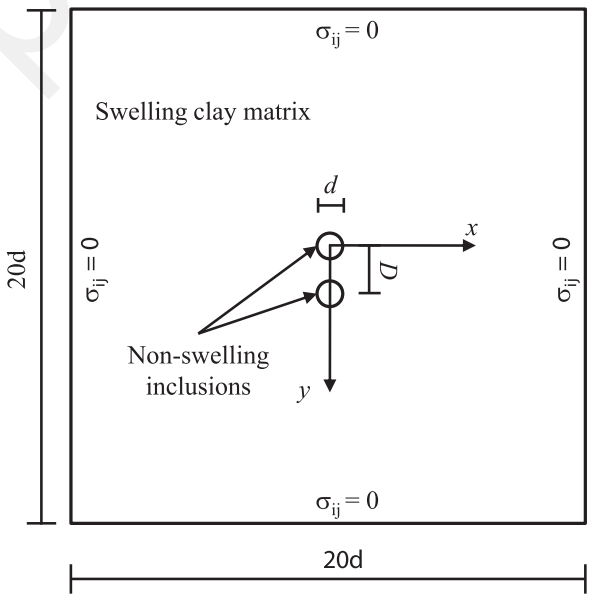

Figure 5. Geometry of the specimen with two cylindrical inclusions.

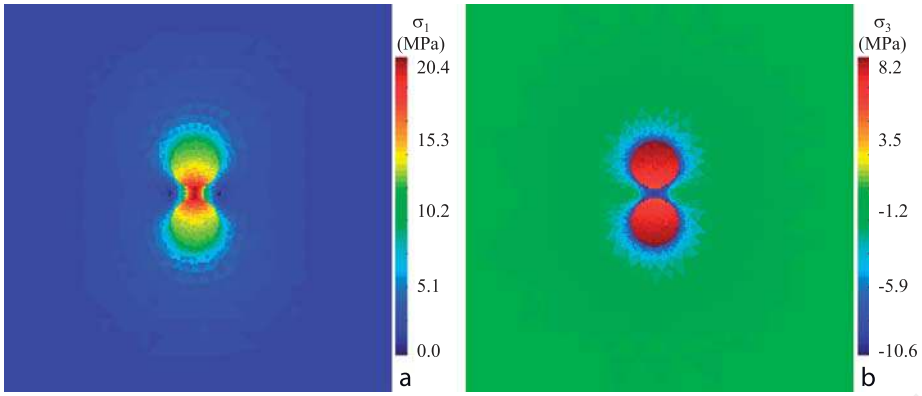

Figure 6. Stress maps around two inclusions in a free-swelling matrix ($D = 1.2d$).

respectively 20.4 and 8.2 MPa, compared with 7.7 MPa for the one inclusion case. The maximum tension is located at the front side of the inclusion, and it decreases gradually to the rear side.

The σ_{yy} profiles along the y axis for various D values are presented in Figure 7. When the two inclusions are sufficiently distant from each other (for example, $D = 4d$), the uniform stress field in the inclusion, corresponding to the theoretical value for a single inclusion, is well found. The interaction between inclusions, when they get closer, leads to an amplification of the stress field. This amplification effect is more pronounced in the front side between two inclusions: It attains 20.4 MPa when $D = 1.2d$, which is nearly three times that for the single inclusion case (7.7 MPa).

As a summary, the local stress induced by the inclusion–matrix interaction is strongly intensified by the interaction between the inclusions, and this amplification effect becomes greater when they get closer. One can derive that the magnitude of local stress increases with the volume fraction of inclusions. In other words, the microcracking occurs more easily in inclusion-rich zones.

3.3. A hemispherical inclusion outcropping at free surface during humidification process

The two previous cases concern the internal stress field generated by a given homogeneous swelling/shrinking of the clay matrix. This corresponds to the steady stage of humidification/desiccation, but the role of self-restraint in the transient stage is not considered. These two types of restrain effects (inclusion–matrix interaction and self-restraint effect) will be considered together in this section. Besides, the experimental observation is usually conducted at the specimen surface. This involves a free surface effect, which will also be studied in this modelling.

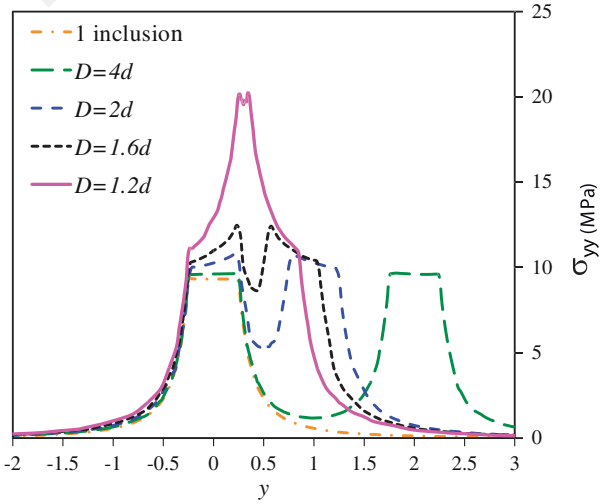

Figure 7. Stress profiles for the two inclusions with different distances.

Consider a hemispherical inclusion outcropping at the free surface of a clay formation. The thickness of the specimen is 3 mm, while the sizes in two other dimensions are infinite. Such specimen, with initial saturation $S_l^0 = 0.66$ ($RH^0 = 80\%$), undergoes a humidification from its free surface side $RH^1 = 90\%$ ($S_l^1 = 0.80$). No external mechanical loading is applied on the specimen. This problem exhibits axial symmetry, so the cylindrical coordinates are used. The configuration of the specimen and boundary conditions are presented in Figure 8. The size in *r*-direction (six times the radius of the inclusion) is large enough to represent the field condition as an infinite boundary. It is stressed that the hemispherical inclusion and the axisymmetrical condition in the present analysis are different from the cylindrical inclusion and plane stress condition for the former cases.

To consider the two effects, the modelling is divided into two parts. The moisture transport process is firstly modelled to determine the evolution of local saturation (Eqn 5). Once the local saturation is known, the local free swelling of the clay matrix can be estimated from Eqn 4, and the internal stress field within the specimen induced by the two restraint effects is then calculated. The local stress may alter the microstructure of the specimen, leading to variation of permeability. Nevertheless, this coupled effect is ignored in this modelling for simplicity.

3.3.1. Humidification process. The humidification process of argillaceous rocks is modelled by Porofis. It is reasonably assumed that the clay matrix is permeable, whereas the inclusion is impermeable. An instantaneous RH increase is applied on the free surface. The evolution of the saturation fields for different moments is presented in Figure 9, which exhibits a quasi-1D humidification process. The moisture gradually penetrates from the top of the specimen to the bottom side. The penetration front is somewhat horizontal, unless it is locally disturbed by the impermeable inclusion.

3.3.2. Internal stress field. Once the saturation distribution for a given moment is assessed, the stress field is then calculated by Porofis in the context of elasticity. The stress maps around the inclusion are presented for two representative moments: the beginning of humidification t = 10 s (Figure 10) and the steady state (Figure 11). It is stressed that, in Figure 10, the extreme value of the stress inside the inclusion near the free surface as a result of singularity (discussed in detail later) is not considered, so no colour is shown is such zones. This scale setting adjustment allows presenting more evidently the internal stress field around the inclusion. Moreover, the normal and shear stresses along the inclusion–

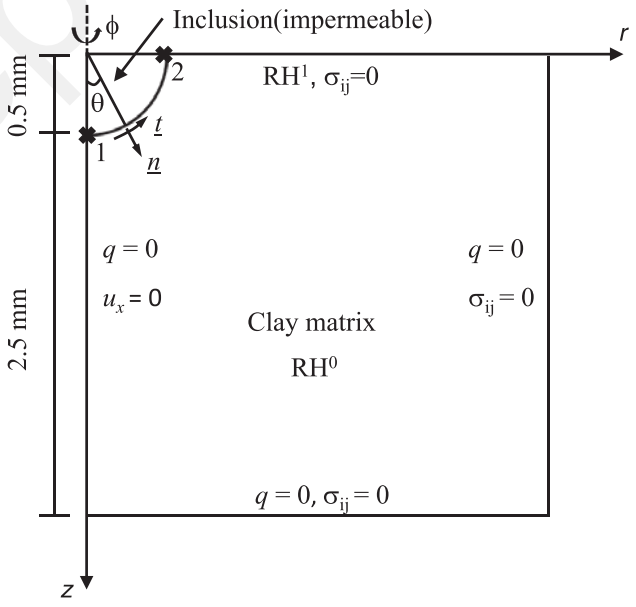

Figure 8. Geometry of the specimen with a hemispherical inclusion outcropping at the free surface.

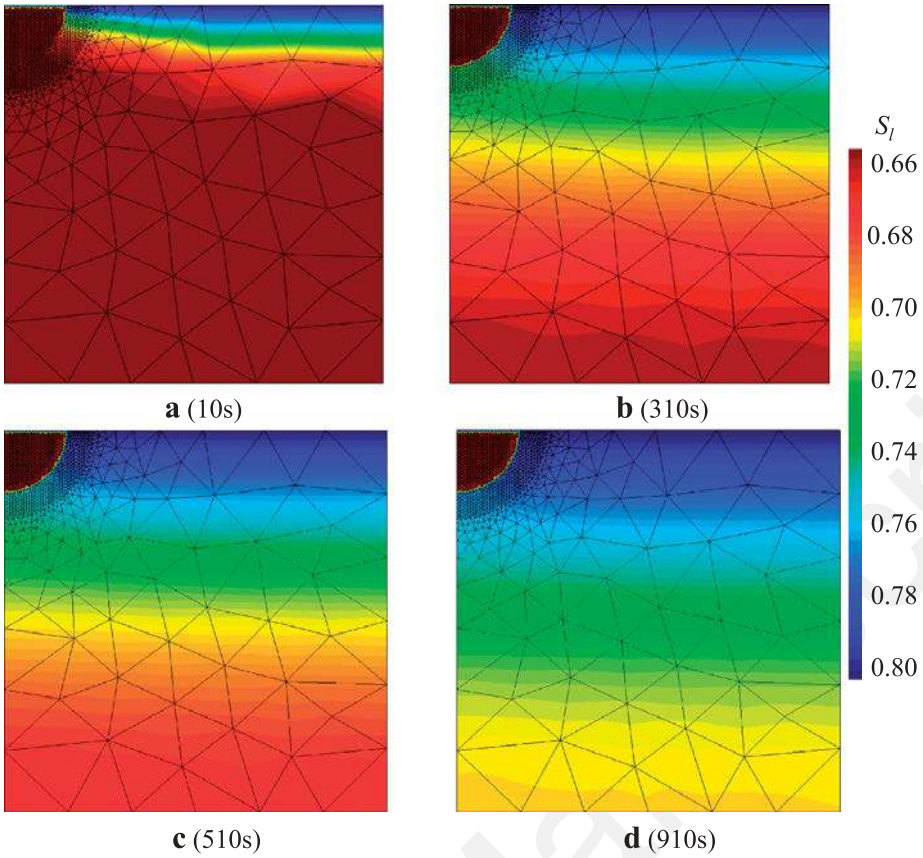

Figure 9. Evolution of saturation within the specimen during a moisture transport process.

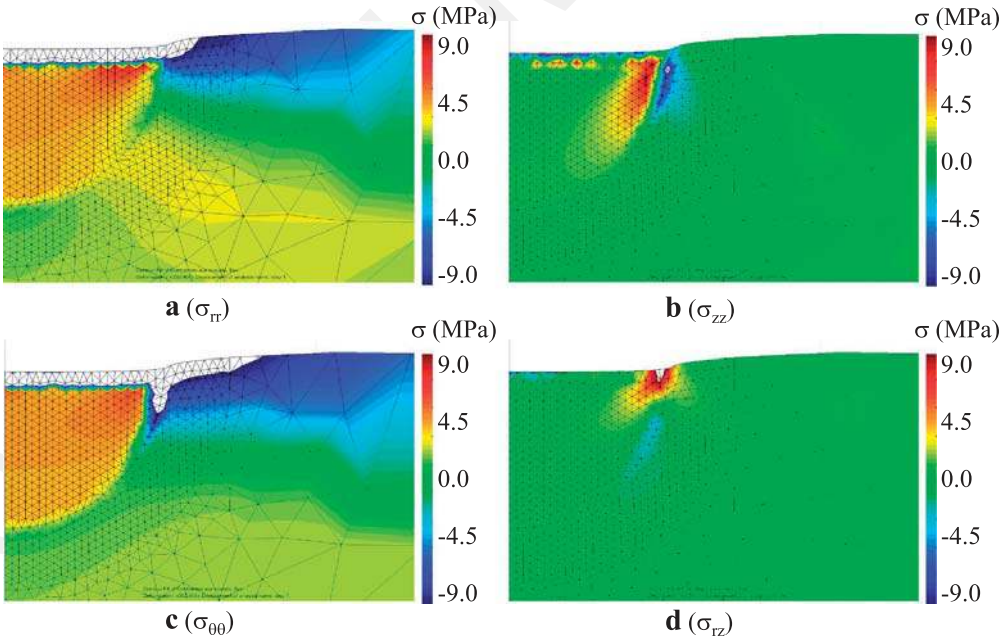

Figure 10. Local stress fields at 10 s.

matrix interface are calculated, shown in Figure 12. Be reminded that for the geometry defined in Figure 8, the normal and shear stresses are related to cylindrical coordinate stresses by the following formulas:

$$\sigma_n = \sigma_{rr}\, sin^2\theta + \sigma_{zz}\, cos^2\theta + \sigma_{rz}\, cos\theta sin\theta \tag{9}$$

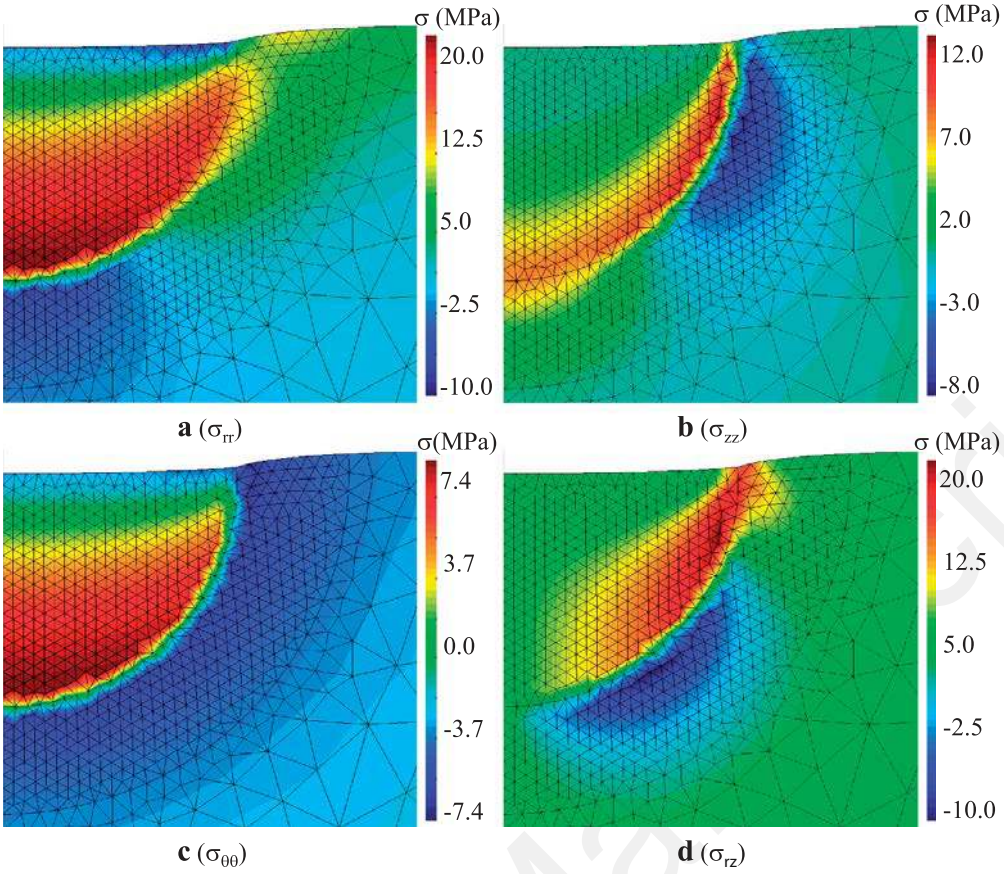

Figure 11. Local stress fields at the steady stage.

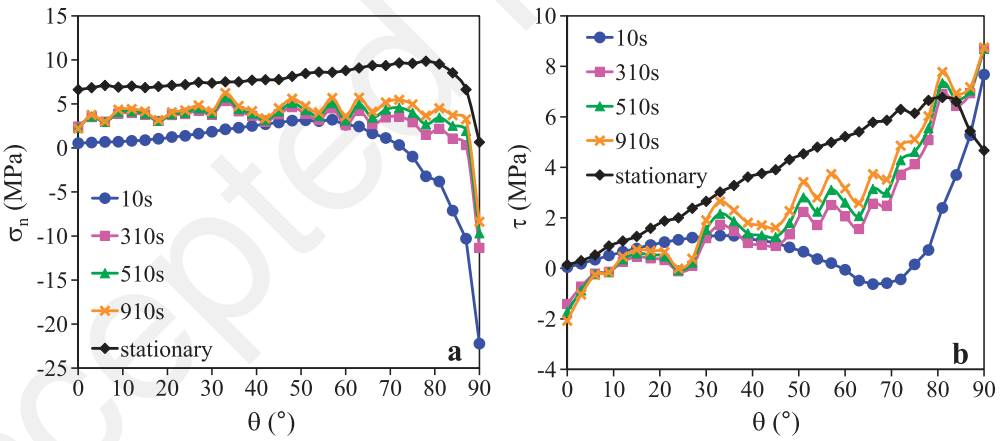

Figure 12. Evolution of stress along the inclusion–matrix interface.

$$\tau = (\sigma_{zz} - \sigma_{rr})cos\theta sin\theta + \sigma_{rz}\left(sin^2\theta - cos^2\theta\right) \tag{10}$$

3.3.2.1. At transient stage. At $t = 10$ s, humidification only occurs at the vicinity of the free surface (Figure 9a). Some compressive local stresses are found at the surface zone of the clay matrix near the inclusion (refer to σ_{rr} and $\sigma_{\theta\theta}$ in Figure 10). The maximum attains more than 9.0 MPa at the inclusion boundary. The stress in the inclusion is mostly tensile (about 4.5 MPa), unless the free surface zone is compressive (more than 9.0 MPa). The normal stress along the interface is null at point 1, while it becomes compressive when approaching the free surface, and increases steeply to its maximum at point 2 (Figure 12). Point 1 is the inclusion bottom ($\theta = 0°$), while point 2 is the

inclusion boundary at the free surface ($\theta = 90°$). The shear stress at the interface is null near point 1, prior to reaching the maximum at point 2. Compared with the two previous studies, one remarkable difference of this analysis consists in emerging shear stresses close to the free surface: It tends to pull out of the inclusion from the free surface (refer to the definition of shear stress in Figure 8). This implies that the potential microcracking is not only in mode I (opening mode induced by tensile stress): It can also be in mode II (sliding mode induced by shear stress).

It should be noted that point 2 is a singular point: The free surface requires the shear stress at this point being null ($\sigma_{rz} = \sigma_{zr} = 0$) whereas the material heterogeneity results in shear stress at the inclusion–matrix interface. In fact, when dissimilar materials are in contact along a surface, localized stress singularities will be found around the points where the contact surface meets a free surface (like point 2). In such case, the stress and strain values tend to become infinite when approaching the singular point. Nevertheless, the simulation based on a finite element method always provides a finite value. This is because the finite element method assesses quantities at the integration point inside elements, but singular points are always mesh nodes that are located at the element edge. Hence, the stress is never calculated at the singular point, and the infinite value cannot be found to determine the singularity. The magnitude of this finite stress at a singular point will be intensified by refining the mesh around it. The order of the stress singularity at the triple contact point depends on wedge angles and materials' properties [20, 21].

As the humidification process goes on, the profile of the normal stress at the interface shifts upwards entirely (Figure 12): It becomes mostly tensile and gradually increases over time, while the compression near point 2 decreases. The shear stress at the interface increases from the bottom (point 1) to the free surface (point 2), and point 2 invovles always the highest shear stress.

3.3.2.2. At the steady stage. From Figure 9, the specimen is not totally humidified yet at 910 s. To study the stress field at the steady state, a uniform free strain that corresponds to the final RH variation is applied to the clay matrix. At the steady stage, the radial stress σ_{rr} in the inclusion does not evolve horizontally, whereas it varies with depth: The maximum is close to the inclusion bottom (the value being 19.7 MPa) and then decreases gradually up to the free surface (Figure 11a). Concerning the matrix, the radial stress is compressive around the bottom of the inclusion, while it becomes tensile near the free surface with the maximum of 8.6 MPa. The axial stress σ_{zz} is generally concentrated along the inclusion boundary: It is tensile in the inclusion, while it is compressive in the matrix. Its maximum is found near point 2.

The normal stress at the inclusion–matrix interface is 6.6 MPa at the inclusion bottom ($\theta = 0°$); then, it increases gently until its maximum is 9.9 MPa at $\theta = 78°$, prior to a sharp decrease to 0.6 MPa at point 2. The shear stress is null at point 1, which can be explained by the symmetry. It increases linearly to the maximum of 6.8 MPa, prior to a steep fall to 4.7 MPa at point 2. Recall that point 2 is a singular point: The shear stress σ_{rz} should attain its maximal at the right vicinity of point 2, whereas the free surface condition requires $\sigma_{zr} = 0$ at point 2 (Figure 12). The value of 4.7 MPa is an approximate evaluation by the finite element numerical simulation. Virtually, the maximal shear stress, deduced by extension of the linear evolution, will be about 7.7 MPa at the right vicinity of point 2, prior to a sharp fall to 0 at point 2. Because of this shear stress, point 2 is always a dangerous point in both transient and steady stages. It is, however, stressed that the normal stress is compressive at the transient stage, while it is tensile at the steady state. This means if the cracking of the interface obeys Mohr–Coulomb's law, then the steady state is the most critical stage in case of humidification, whereas the initial transient stage ($t = 0$) is the most critical stage in case of desiccation.

3.3.3. Self-restraint effect at the transient stage (without an inclusion). The normal stress near point 2 is subjected to a sign change during the humidification process: It is highly compressive at the beginning, whereas it becomes slightly tensioned at the steady state. This phenomenon is evidently attributable to the self-restraint effect: The moisture gradient during the transient stage leads to internal stresses within the specimen. Certainly, the self-constraint effect is generally combined with inclusion–matrix interaction (as in the previous section). To better understand the contribution of self-restraint effect, the domain of the inclusion is considered as a hole (the stiffness is null) to exclude the effect of inclusion–matrix interaction. The stress field for the 10-s step is recalculated and presented in Figure 13. The 10-s step is

chosen because the self-restraint effect is greatest (the moisture gradient is at maximum) at the beginning of the humidification process (refer to the saturation gradient in Figure 9). High compressive stresses (with the maximum of 12.0 MPa) are found at the wetting surface, while the moderate tension with the maximum of 3.0 MPa occurs at its lower part.

To have a better understanding of the self-restraint effect, consider a simple case of a rectangular specimen undergoing a one-side humidification from its top to the bottom. At the beginning, the upper part of the specimen is firstly humidified and tends to swell. However, this swelling will be restrained by the non-swelling bottom part where the humid moisture has not reached. Such self-restraint effect results in compression at the top part and tension at the bottom part. When the moisture transport goes on and the free swelling becomes more homogeneous inside the specimen,

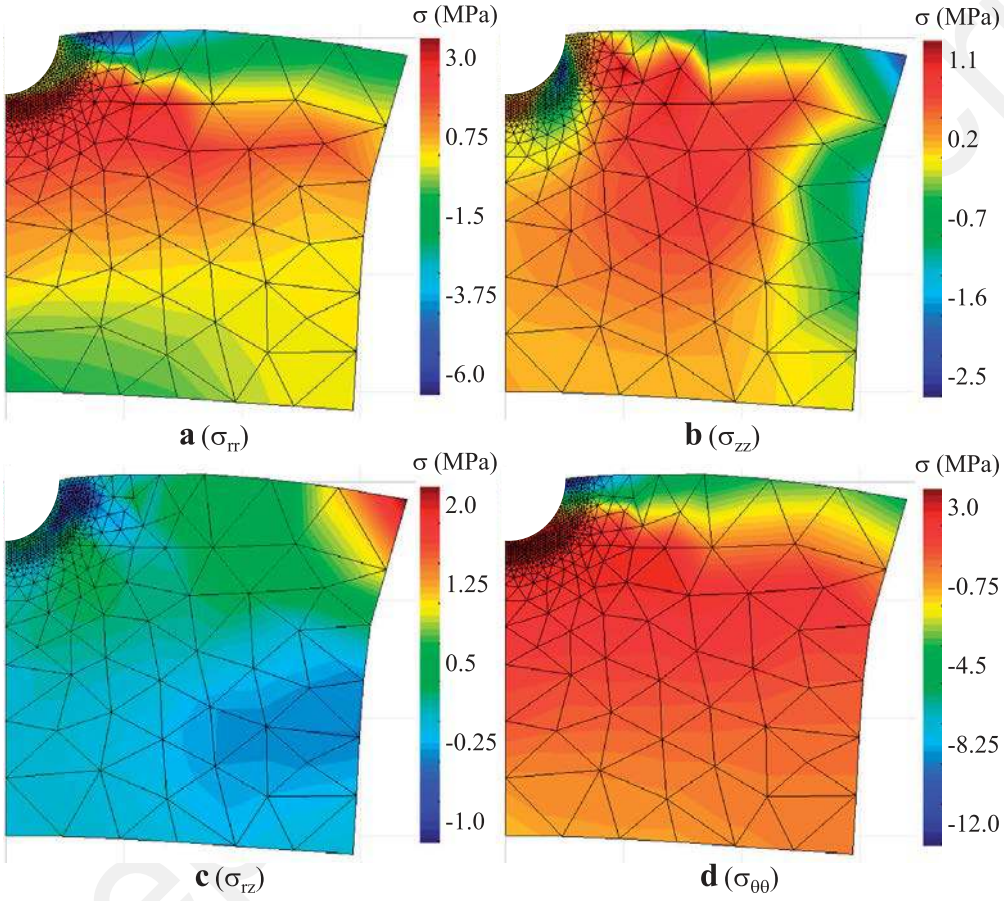

Figure 13. Local stress fields at 10 s (without an inclusion).

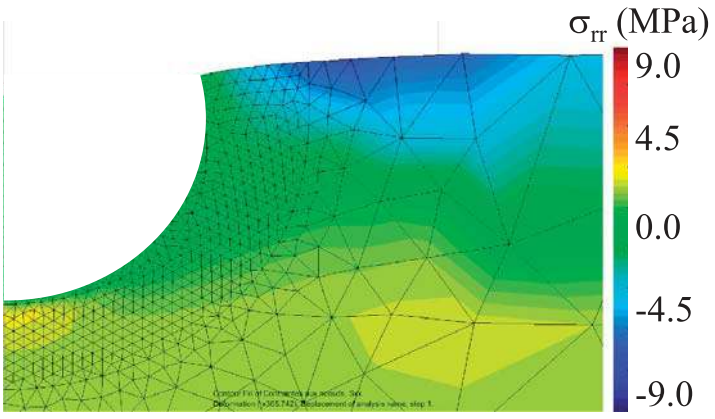

Figure 14. Radial stress filed at 10 s for the case without an inclusion.

the stress induced by the self-restraint effect gradually decreases and finally vanishes at the steady state. That is why the compression at the neighbouring zone of point 2 decreases with time. The stress induced by the self-restraint effect at the hydric loading surface is compressive for the swelling (humidification) case, whereas it is tensile for the shrinking (desiccation) case.

The radial stress filed at 10 s for the case without an inclusion is zoomed and rescaled (Figure 14) to be compared with the case with an inclusion (Figure 10a). In general, the radial stress is more intense

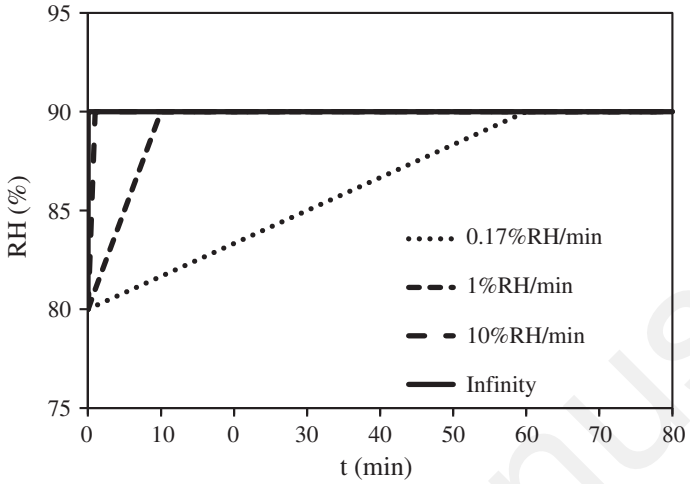

Figure 15. Different hydric loading rates.

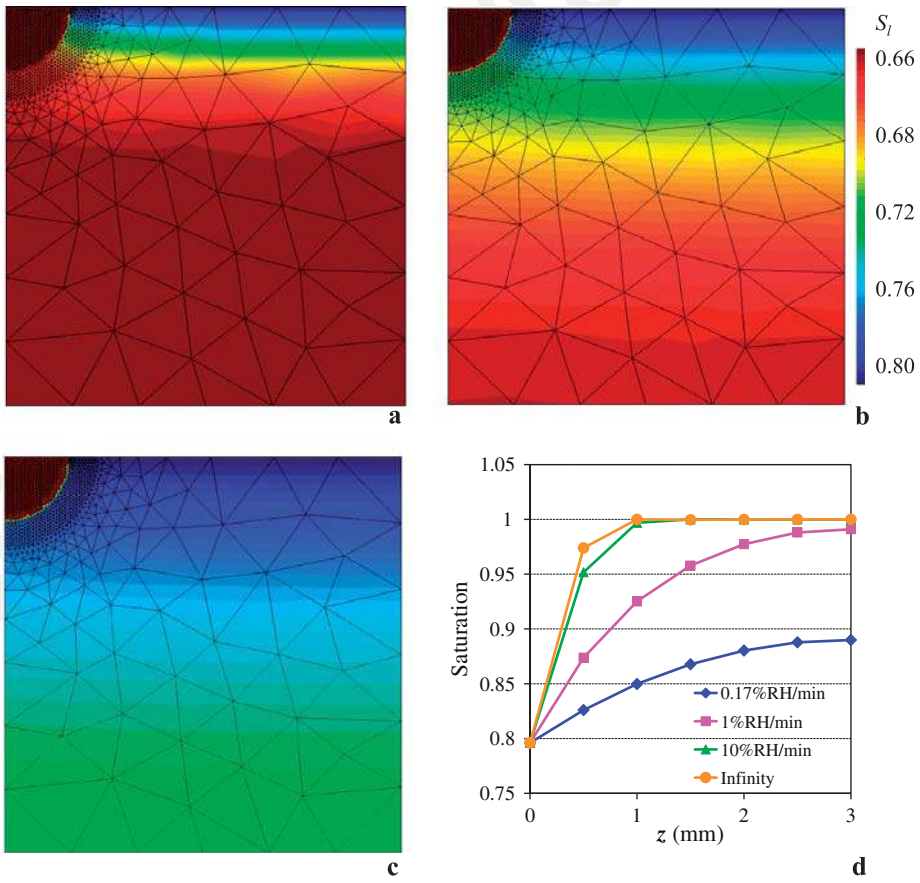

Figure 16. Saturation distribution inside the specimen at the time of 10 s after the end of hydric loading: (i) 70 s for the 10% RH/min case, (ii) 610 s for the 1% RH/min case, (iii) 3610 s for the 0.17% RH/min case, and (iv) saturation gradients from top ($z = 0$) to bottom ($z = 3$ mm) of a specimen far away from the inclusion ($r = 3$ mm) for different cases.

with the inclusion: The maximum is 32 MPa (at point2), whereas the maximal compression is 6 MPa for the case without an inclusion. Actually, the non-swelling inclusion hinders the displacement of point 2 because of free swelling (shrinking) and intensifies the stress because of self-restraint: compression (tension) in case of humidification (desiccation). Note that this amplification effect of the inclusion for self-restraint is opposite to its role for the inclusion–matrix interaction: tension (compression) for the humidification (desiccation) case. The total stress is indeed a sum of the two effects (inclusion–matrix interaction and self-restraint). For each effect, the maximal stress is always found at the interface. However, the two effects lead to opposite sign stresses so that the total stress field is very complex: Its maximum might not be at the interface.

3.3.4. Effect of hydric loading rate. The experimental results have revealed that the damage of argillaceous rocks induced by humidification/desiccation is strongly controlled by the hydric loading rate [6]. The hydric loading rate plays an important role for the stress induced by self-restraint, and this effect will be studied in this section (refer to four different rates in Figure 15). The saturation distributions at 10 s after the end of the hydric loading (10% RH) are estimated (Figure 16). This means $t = 3610$ s for the 0.17% RH/min rate, 610 s for the 1% RH/min rate, 70 s for the 10% RH/min rate, and 10 s for the instantaneous hydric loading case. The maximal saturation gradient increases with the hydric loading rate. The comparison of stress is concentrated at point 2 at the free surface, where a considerable portion of the local stress is attributed to the self-restrain effect. Its evolution at the beginning of humidification is plotted in Figure 17. The stress at point 2 increases linearly during the stage of hydric loading and attains its maximum once the RH variation finishes. Then, the normal stress gradually decreases, whereas its shear stress remains constant. The stress at point 2

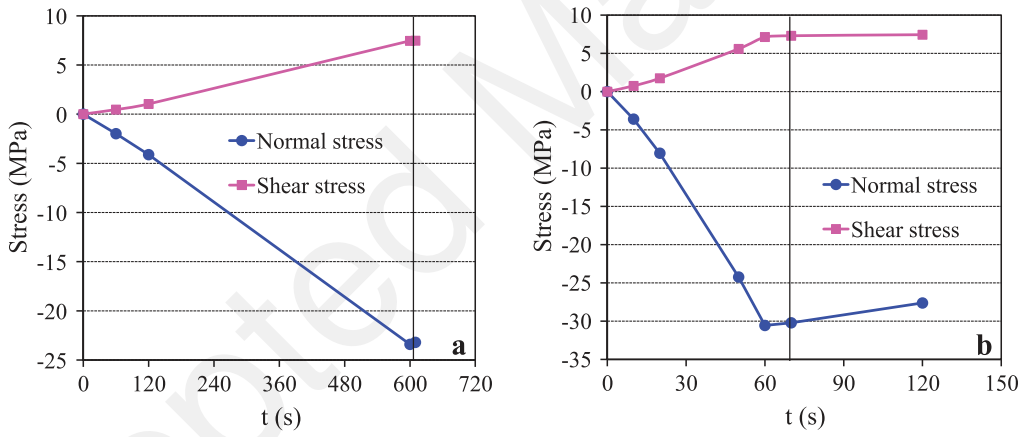

Figure 17. Stress evolution at point 2 during hydric loading in case of (i) 1% RH/min and (ii) 10% RH/min.

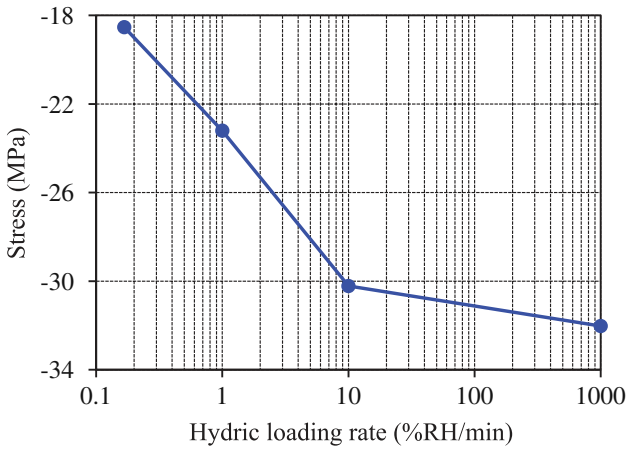

Figure 18. Normal stress at point 2 at the time of 10 s after the end of hydric loading versus hydric loading rate.

for the observation instant (10 s after the end of hydric loading) is drawn versus the hydric loading rate: Its value is 18 MPa in case of 1% RH/min, while it attains 32 MPa in case of instantaneous hydric loading (as shown in Figure 18). This difference is essentially related to variation of the saturation gradient for different hydric loading rates: The gradient becomes steeper when the hydric loading increases, and the stresses induced by self-restraint consequently become more important.

4. CONCLUSION

When the RH varies, an internal stress field is generated inside argillaceous rocks because of two terms: inclusion–matrix interaction and self-restraint. The clay matrix undergoes a volume change because of its specific swelling–shrinking properties, but the inclusions restrain this free deformation, and local stresses are generated. Meanwhile, the moisture gradient developed within the specimen during a humidification/desiccation process leads to non-uniform swelling/shrinking strains, which also contribute to the internal stress field. The internal stress field is responsible for the damage phenomena in argillaceous rocks.

The internal stresses induced by the two effects are investigated by analytical and numerical methods. For self-restraint, the moisture gradient results in tensile stresses at the desiccation (shrinking) surface but in compressive stresses at the humidification (swelling) surface. Such type of stresses is maximal at the beginning of humidification/desiccation processes, prior to a decreasing stage when the moisture transport goes on. The tensile stress for the desiccation case may lead to microcracks perpendicular to the drying surface, which can be observed for a wide range of shrinking materials. The stress induced by self-restraint strongly depends on the hydric loading rate: It increases with the hydric loading rate.

The inclusion–matrix interaction in argillaceous rocks results in tensile stress in the inclusion for the humidification case (swelling clay matrix) and compressive stress for the desiccation case (shrinking clay matrix). The microcracking exhibits dissimilar patterns in different cases: Separation of inclusion–matrix interface may be found in the humidification case, whereas desiccation potentially results in radial microcracks as well as shear microcracks in the matrix. Moreover, neighbouring inclusions will perturb and intensify the internal stress field, and this amplification effect increases when the neighbouring inclusion gets closer. It should be noted that the inclusions play opposite roles for the two effects: It amplifies the stress because of self-restraint effect (i.e. compression for the humidification case and tension for the desiccation case), while the inclusion–matrix interaction leads to tension in case of humidification and compression in case of desiccation.

A case of a single inclusion outcropping at a free surface is considered to study the effect of the free surface. Regardless whether humidification or desiccation occurs, the inclusion–matrix interface near the free surface is a dangerous location for damage because of high shear stresses. For example, this point undergoes tensile stresses combined with high shear pulling the inclusion out of the matrix in the humidification case. Moreover, the normal stress at the interface approaching the free surface undergoes a sign change during the moisture transport process: It is compressive at the beginning of the humidification process mainly because of self-restraint, while it is tensile at the end of this process because the inclusion–matrix interaction effect becomes predominant. This demonstrates that the self-restraint and inclusion–matrix interaction should be taken into account together, and the total stress is indeed the result of these two effects.

APPENDIX

The governing equations for a cylindrical inclusion embedded in an infinite-swelling matrix are

Equilibrium equation

$$\frac{d\sigma_{rr}}{dr} + \frac{\sigma_{rr} - \sigma_{\theta\theta}}{r} = 0 \tag{A-1}$$

where σ_{rr} and $\sigma_{\theta\theta}$ denote the radial and orthoradial stresses, respectively, while r denotes the radial coordinate.

Strain-displacement relation

$$\varepsilon_{rr} = \frac{du}{dr}, \qquad \varepsilon_{\theta\theta} = \frac{u}{r} \tag{A-2}$$

where ϵ_{rr}, and $\epsilon_{\theta\theta}$ denote the radial and orthoradial strains, while u is the radial displacement only depending on r.

Constitutive equation

For the inclusion,

$$\varepsilon_{rr} = \frac{1}{E_i}(\sigma_{rr} - \nu_i\sigma_{\theta\theta}) \tag{A-3a}$$

$$\varepsilon_{\theta\theta} = \frac{1}{E_i}(\sigma_{\theta\theta} - \nu_i\sigma_{rr}) \tag{A-3b}$$

$$\varepsilon_{zz} = \frac{-\nu_i}{E_i}(\sigma_{\theta\theta} + \sigma_{rr}) \tag{A-3c}$$

For the matrix with free deformation $\boldsymbol{\varepsilon}^h$,

$$\varepsilon_{rr} = \frac{1}{E_m}(\sigma_{rr} - \nu_m\sigma_{\theta\theta}) + \varepsilon^h \tag{A-4a}$$

$$\varepsilon_{\theta\theta} = \frac{1}{E_m}(\sigma_{\theta\theta} - \nu_m\sigma_{rr}) + \varepsilon^h \tag{A4-b}$$

$$\varepsilon_{zz} = \frac{-\nu_m}{E_m}(\sigma_{\theta\theta} + \sigma_{rr}) + \varepsilon^h \tag{A4-c}$$

where E and v denote Young's modulus and Poisson's ratio. The subscripts i and m represent the inclusion and the matrix, respectively. Note that the constitutive equations are based on the hypothesis of plane stress condition: Vertical stress is null ($\sigma_{zz} = 0$).

The combination of the previously mentioned equations gives the following equation that holds not only for the inclusion but also for the matrix:

$$\frac{d^2u}{dr^2} + \frac{1}{r}\frac{du}{dr} - \frac{u}{r^2} = 0 \tag{A-5}$$

The general solution of the previous equation is

$$u = Ar + \frac{B}{r} \tag{A-6}$$

where A and B are two constants that can be determined by the boundary conditions. For the inclusion, $B = 0$ as $u(0) = 0$ because of the symmetry. Therefore, the strain and stress are uniform in the inclusion and can be expressed as

$$\varepsilon_{rr} = \varepsilon_{\theta\theta} = A_i \tag{A-7a}$$

$$\sigma_{rr} = \frac{E_i}{1 - \nu_i}A_i \tag{A-7b}$$

The strain and stress in the matrix are

$$\varepsilon_{rr} = A_m - \frac{B_m}{r^2}, \quad \varepsilon_{\theta\theta} = A_m + \frac{B_m}{r^2} \tag{A-8a}$$

$$\frac{1 - {\nu_m}^2}{E_m}\sigma_{rr} = (1 + \nu_m)\left(A_m - \varepsilon^h\right) - (1 - \nu_m)\frac{B_m}{r^2} \tag{A-8b}$$

Because the stress at infinity should be null $\sigma_{rr}(\infty) = 0$, then

$$A_m = \varepsilon^h \tag{A-9}$$

The assumption of perfect adhesion at the inclusion–matrix interface and so the continuity of the displacement at this interface ($|r1 = |$) yields

$$A_i = \varepsilon^h + \frac{B_m}{R^2} \tag{A-10}$$

B_m can be determined from the continuity of the normal stress at the inclusion–matrix interface:

$$B_m = \frac{-R^2\varepsilon^h}{1 + (1 - \nu_i)E_m/(1 + \nu_m)E_i} \tag{A-11}$$

Finally, the uniform stress in the inclusion is found:

$$\sigma_{rr} = \frac{\varepsilon^h}{(1 - \nu_i)/E_i + (1 + \nu_m)/E_m} \tag{A-12}$$

REFERENCES

1. Shao JF, Ata N, Ozanam O. Study of desaturation and resaturation in brittle rock with anisotropic damage. *Engineering Geology* 2005; **81**:341–352.
2. Pichler B, Cariou S, Dormieux L. Damage evolution in an underground gallery induced by drying. *International Journal for Multiscale Computational Engineering* 2009; **7**:65–89.
3. Bemer E, Longuemare P, Vincké O. Poroelastic parameters of Meuse/Haute Marne argillites: effect of loading and saturation states. *Applied Clay Science* 2004; **26**:359–366.
4. Hoxha D, Giraud A, Homand F, Auvray C. Saturated and unsaturated behaviour modelling of Meuse-Haute/Marne argillite. *International Journal of Plasticity* 2007; **23**:733–766.
5. Maleki K, Pouya A. Numerical simulation of damage–permeability relationship in brittle geomaterials. *Computers and Geotechnics* 2010; **37**:619–628.
6. Wang LL. Micromechanical experimental investigation and modelling of strain and damage of argillaceous rocks under combined hydric and mechanical loads. PhD thesis, Ecole Polytechnique, Palaiseau, France, 2012.
7. Zhang CL, Rothfuchs T. Experimental study of the hydro-mechanical behaviour of the Callovo-Oxfordian argillite. *Applied Clay Science* 2004; **26**:325–336.
8. Bisschop J, van Mier JGM. Effect of aggregates on drying shrinkage microcracking in cement-based composites. *Materials and Structures* 2002; **35**:453–461.
9. Mihai IC, Jefferson AD. A material model for cementitious composite materials with an exterior point Eshelby microcrack initiation criterion. *International Journal of Solids and Structure* 2011; **48**:3312–3325.
10. Jagla EA. Stable propagation of an ordered array of cracks during directional drying. *Physical Review E* 2002; **65**:046147.
11. Jenkins DR. Optimal spacing and penetration of cracks in a shrinking slab. *Physical Review E* 2005; **71**:056117.
12. Jenkins DR. Determination of crack spacing and penetration due to shrinkage of a solidifying layer. *International Journal of Solids and Structure* 2009; **46**:1078–1084.

13. Timm DH, Guzina BB, Voller VR. Prediction of thermal crack spacing. *International Journal of Solids and Structure* 2003; **40**:125–142.
14. Laird DA. Influence of layer charge on swelling of smectites. *Applied Clay Science* 2006; **34**:74–87.
15. Wang LL, Bornert M, Chanchole S, Héripré E, Yang DS, Halphen B, Pouya A, Tanguy A, Caldemaison D. Micro-scale experimental investigation of the anisotropic swelling of COx argillaceous rocks. *Clay Minerals* 2013; **48**:391–402.
16. Coussy O. Mechanics and physics of porous solids. John Wiley & Sons, Ltd: Chichester, 2010.
17. Mainguy M, Coussy O, Baroghel-Bouny V. Role of air pressure in drying of weakly permeable materials. *Journal of Engineering Mechanics* 2001; **127**(6):582–592.
18. ANDRA. Référentiel du Site Meuse/Haute-Marne: Tome 2, 2005.
19. Wang LL, Bornert M, Chanchole S, Héripré E. Experimental investigation of the free swelling of crushed argillite. *Geotechnique Letters* 2013; **3**(2):89–92.
20. Sator C, Becker W. Closed-form solutions for stress singularities at plane bi- and trimaterial junctions. *Archive of Applied Mechanics* 2012; **82**:643–658.
21. Tadanobu I, Masaki H, Shojiro O. Disappearance conditions of thermal stress singularities based on stress intensity in two and three-phase bonded structures. *International Journal of Fracture* 1999; **96**:179–201.